Low Complexity Joint Radar-Communication Systems Design in the RF Domain

Christos G. Tsinos, *Senior Member, IEEE,* Aryan Kaushik, *Member, IEEE,* Aakash Arora, *Member, IEEE,* Christos Masouros, *Fellow, IEEE,* Fan Liu, *Member, IEEE,* and Symeon Chatzinotas, *Fellow, IEEE*

***Abstract*—In this paper, we propose an efficient and low hardware complexity multiuser multiple-input multiple-output (MU-MIMO) joint radar-communication (JRC) system. The proposed system is implemented via an analog phase shifting network and a variable gain amplifier. The proposed system simultaneously supports the downlink communication with multiple users and radar target detection through its multiple antenna transmitter. We consider two design architectures for the phase shifting network: infinite and finite resolution phase-shifters. Furthermore, the energy consumption of the both the proposed architectures is modeled. For these two cases, the transmit waveform is designed in the radiofrequency (RF) domain such that the downlink multi-user interference is minimized while the desired radar beampattern is achieved under architecture specific constraints. To do so, a difficult nonconvex optimization problem is formulated and solved by a novel algorithmic solution based on the primal-dual framework. The numerical results verify the good performance and significant gains in the energy efficiency of the proposed approach with respect to the existing state-of-the-art fully-digital methods.**

***Index Terms*—Joint radar-communications, MU-MIMO, low hardware complexity, waveform design, phase shifter, primal-dual, RF precoding.**

I. Introduction

THE sixth Generation (6G) wireless technologies have to satisfy an exponentially increasing demand for high quality wireless communications services, since a huge volume of different devices demand access to the wireless medium. By 2023, 29.3 billion interconnected devices [1] were expected, spanning from regular cellular networks to small-scale smart devices within the context of the so-called "Internet of Things (IoT)" [2], [3]. Therefore, wireless communication systems could benefit from additional frequency spectrum resources, in order to meet those demands. Towards that direction, the efficient utilization of the currently occupied electromagnetic spectrum by other applications, is a high potential solution. Among different proposals [4]- [5], the case of joint communications-radar spectrum sharing has recently gained great interest in the literature [6]- [7]. The latter is usually implemented via two different approaches: 1) Coexistence of the radar and the communication systems [8]- [10], and 2) Joint radar-communication (JRC) system design that simultaneously supports both functions [11]- [16].

In the present paper, we are interested in JRC systems aiming at designs that can jointly handle the operations of both the radar and communication systems. Such designs may apply in real-time joint sensing/communication operations via a single hardware setup. Thus, they require lesser hardware complexity, implementation costs and communication overhead in comparison to the coexistence-based approach [8]- [10]. This is the case since in the coexistence-based approach, the communication and radar systems are, in general, implemented in different hardware platforms. Furthermore, the two systems require to exchange information related to the interference channels and radar waveform parameters to manage the cross interference between them [8]- [10].

In the considered regime, the JRC system is implemented by designing the transmit waveform such that both the performance of the radar and communication systems is optimized subject to spatial/temporal constraints. Following this approach, the available spatial degrees of freedom in the JRC system are effectively exploited, i.e., via multiple transmit antennas. As a result, the designed transmit waveform for such a JRC MIMO system achieves high information transmission rates to the intended users and a reliable operation of the radar system.

A. Prior State-of-the-Art

In [11], the transmit waveform for the JRC system is designed by minimizing the multiuser interference such that a desired radar beampattern is achieved via imposing a specific structure on the covariance matrix of the transmit signals. In [12], the problem of joint transmit waveform and receive filter design under different spatial/temporal constraints is studied. In [13], linear precoding solutions were derived such that the designed signals to be transmitted match the desired radar beampattern, satisfy a specified signal-to-interference ratio (SINR) level at the intended users and a transmit power

Christos G. Tsinos is with the Department of Digital Industry Technologies, National and Kapodistrian University of Athens, Greece (e-mail:ctsinos@uoa.gr).

Aryan Kaushik is with the Department of Computing and Mathematics, Manchester Metropolitan University, UK. (E-mail: a.kaushik@ieee.org).

Aakash Arora is with the Centre for Applied Research in Electronics, Indian Institute of Technology Delhi, New Delhi, India (email: aarora@care.iitd.ac.in).

Christos Masouros is with the Department of Electronic and Electrical Engineering, University College London, United Kingdom (e-mail: c.masouros@ucl.ac.uk).

Fan Liu is with the Department of Electrical and Electronic Engineering, Southern University of Science and Technology, China (e-mail:liuf6@sustech.edu.cn).

Symeon Chatzinotas is with SnT, University of Luxembourg, 1855 Luxembourg City, Luxembourg and with College of Electronics & Information, Kyung Hee University, Yongin-si, 17104, Korea (e-mail:symeon.chatzinotas@uni.lu).

constraint, as well. An alternative approach with improved performance was followed in [17] according to which, the linear precoding matrix is decomposed into two parts, one for the communication and one for the radar system.

In the aforementioned works, the JRC system is based on a fully-digital transceiver. Such transceivers present high hardware complexity/power consumption, especially for systems equipped with large-scale/massive antenna arrays. This is due to the one Radio Frequency (RF) chain per-antenna element requirement for the implementation of a fully digital technique. Each RF chain includes a number of different electronic elements among which are the Digital-to-Analog/Analog-to-Digital converters (DACs/ADCs) that are the most complex and energy consuming devices in short range applications [18].

Towards that direction, hybrid analog-digital (A/D) transceivers have been proposed in the wireless communication literature [19]- [24]. Recently, hybrid A/D transceiver solutions for JRC systems have been proposed in [25], [26]. The aim of these approaches is the reduction of the number of the transceiver's RF chains via a two stage beamformer that is constituted by a low dimensional digital precoder applied in the base-band followed by an analog beamformer applied in the RF domain. On the contrary, the reduction on the number of RF chains has impact on the number of the supported streams that can be transmitted simultaneously when a linear precoding technique is employed (i.e., the number of the supported streams can be equal to the number of the available RF chains, at most) [27].

From the previous discussion, it is evident that the reduction on the hardware complexity/power consumption comes at the cost of a transceiver design of limited capabilities compared to its fully digital counterpart. To that end, a solution to design the transmitter mainly from analog components such as Phase Shifters (PS) and a Variable Gain Amplifier (VGA), etc., is proposed in [28]. Through the nonlinear design of the transmit signals, the transmission of multiple parallel streams is enabled and thus, it is able to support efficiently multiuser communication while exhibiting significant gains in power consumption and hardware complexity. Such systems based on analog components have also been recently developed for Orthogonal Frequency Division Multiplexing (OFDM) [29] and cognitive radio systems [30]. Given the limitations posed by modern systems where low hardware complexity and/or battery operated devices ask for wireless connectivity and sensing capabilities (i.e., IoT, cyberphysical systems), transmitters based on phase shifting network-aided analog components is a viable solution.

Furthermore, there are various works in the literature addressing the problem of finite and infinite resolution phase-shifters-based models in communications and radar applications [31]–[33]. The problem of maximizing the spectral efficiency in hybrid beamforming systems employing finite resolution phase-shifters is discussed in [31]. In [32], the problem of binary sequences design with good aperiodic/periodic autocorrelation and cross-correlation functions is considered for MIMO radar systems. Further, the work in [33] considered the problem of beamforming optimization for intelligent reflecting surface (IRS)-aided wireless network by minimizing the transmit power by jointly optimizing the transmit precoding and the discrete phase-shifts at the IRS.

To that end, in the present paper, we are motivated to develop JRC systems based on analog components and study their performance in different regimes. A first study of this approach was presented in [34] where a solution based on infinite resolution PS is presented. In the present work, we provide detailed derivations of the presented solutions, provide an additional problem formulation for a system model based on finite resolution PSs and an algorithmic solution tailored for the latter problem. Furthermore, detailed energy consumption models are derived for both the considered architectures with finite and infinite resolution PSs upon which their energy efficiency is calculated. In addition, the performance of the proposed architectures has been extensively studied through simulations and thoroughly compared to the state-of-the-art solutions for different key model parameters.

B. Contributions

More specifically, the contributions are as follows:

- A novel analog architecture for multiuser (MU)-MIMO JRC system based on a single phase-shifter per antenna and a common variable gain amplifier (VGA) that drives the phase shifting network is proposed. Both the cases of infinite and finite resolution PSs are considered.
- For the proposed system, the optimal transmit waveform is designed by formulating an optimization problem to minimize the communication multiuser interference (MUI) criterion while imposing a specific radar beampattern and also satisfying constraints related to the proposed architecture, i.e., infinite or finite unit-modulus constraints.
- The resulting optimization problems are nonconvex, nondeterministic polynomial time (NP)-hard and have yet to be addressed in literature [35]. To that end, we propose novel efficient algorithmic solutions based on the primal-dual framework [36].
- The power consumption of the new JRC system is modeled in order to enable the evaluation of its energy efficiency defined as the ratio of the achievable sum rate to the power consumed by the JRC system's components.
- The numerical results verify the excellent performance of the MIMO JRC system compared to the state-of-the-art fully-digital approaches while offering significant gains in terms of the power consumption/energy efficiency. Furthermore, it is shown that PS modules of only 1-bit resolution suffice to achieve very close performance to the architecture based on infinite resolution ones.

The rest of the paper is organized as follows: Sec. II presents the system model. In Sec. III, the optimization problems to be solved are formulated and the corresponding algorithmic solutions are developed. Sec. IV presents the power consumption model of the proposed JRC architecture. In Sec. V numerical results are presented and Sec. VI concludes this work.

Notation: **A**, **a**, a: matrix, vector and scalar variable, respectively; tr(·), re(·), $(\cdot)^T$, $(\cdot)^H$, $(\cdot)^{-1}$,$(\cdot)^{-H}$,$\|(\cdot)\|_p$ and $\|(\cdot)\|_F$ denote the trace, real-term, transpose, Hermitian transpose, inverse, inverse Hermitian transpose, p norm and Frobenius norm, respectively; $\mathbf{A}_{i,j}$ and $\mathbf{a}_i$ are the (i,j)-th and i-th elements in $\mathbf{A}$ and $\mathbf{a}$, respectively; $|\cdot|$ is the modulus of a complex number. $\mathbf{I}_N$ is N-size identity matrix; $\mathbb{C}$ and $\mathbb{R}_+$ and denote the set of complex and real positive numbers, respectively; diag$\{\cdot\}$ is the operator that returns the diagonal entries of a matrix in diagonal matrix form; $\mathbb{E}\{\cdot\}$ denotes the expectation operator; $\mathcal{CN}(a,b)$ is a complex Gaussian vector with mean a and variance b.

II. System Model

Let us assume, a MU-MIMO JRC system equipped with a uniform linear array (ULA) of N_{T} antenna elements which simultaneously serves N_{R} single-antenna downlink user terminals (UTs) and transmits radar probing waveforms towards the targets. To reduce the hardware complexity, we propose an analog architecture for the MIMO JRC system as shown in Fig. 1a. Such an architecture is implemented by one phase shifter (PS) module connected to each transmit antenna before the power amplifiers (PAs). Both the cases of infinite and finite resolution PS are assumed. As shown in Fig. 1a, this phase shifting network is driven by a common VGA, with the local oscillator (LO) circuitry, that tunes the common amplitude of the complex output transmit signals.

Different than a typical fully digital architecture (Fig. 1b), this architecture does not require high hardware complexity/high power consumption components such as DACs to be implemented. On the contrary, fully digital architectures require two DACs (one for the real part and one for the complex part of the signal) per antenna array element that exponentially increase the required hardware complexity/power consumption, especially for large-scale antenna arrays.

Moreover, the proposed analog architecture in Fig 1.a, has significant gains on the hardware complexity/power consumption compared to hybrid Analog/Digital (A/D) architectures since it requires only one phase shifting element per array element. Contrariwise, a fully connected hybrid A/D architecture requires $N_{\mathrm{RF}}N_{\mathrm{T}}$ phase shifting elements to interconnect the $N_{\mathrm{RF}} << N_{\mathrm{T}}$ RF chains with the N_{T} antenna array elements. On top of this, two DACs per each one of the employed N_{RF} chains are required [20].

It is also noteworthy to point out that the proposed architecture in Fig.1a enables the nonlinear design of the transmit signals, in contrast to the linear design that both the fully digital and hybrid A/D architectures are based to. The nonlinear design offers a full control on the spatio-temporal characteristics of the digital transmit waveform. The latter comes at the cost of the requirement for updates based on the symbol time basis. This may increase the computational requirements compared to hybrid A/D and fully digital solutions that require updates based on a channel coherence basis, especially in slow-fading channels.

A detailed comparison between fully analog, hybrid A/D and fully digital architectures is given in [28] for communication only systems, though the presented results and conclusions can be also extended to the JRC system model, considered in the present paper.

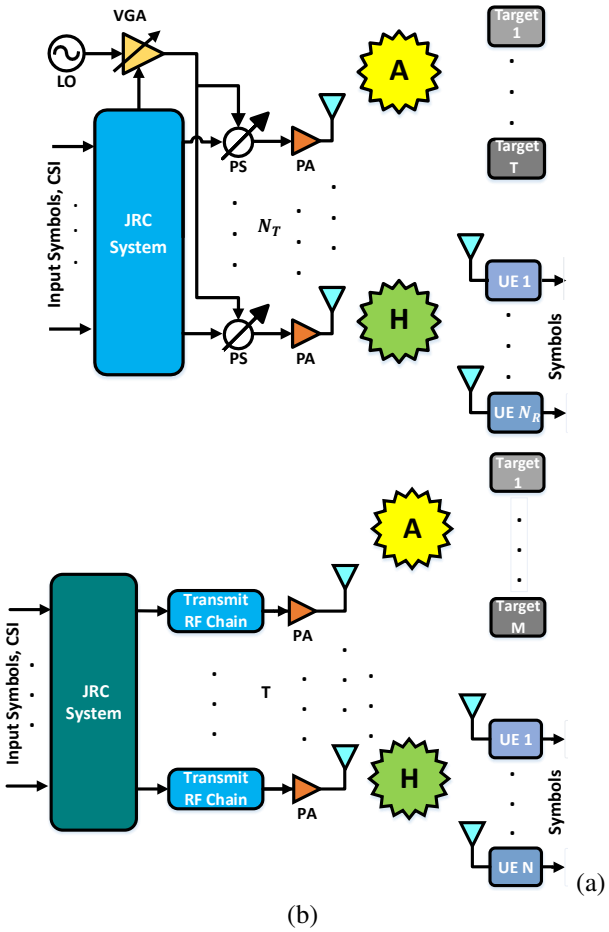

Fig. 1: a) Proposed analog architecture for the MIMO JRC system. b) Fully digital architecture for the MIMO JRC system

A. Communication Model

The received signals of the downlink communication users $\mathbf{Y}$ can be expressed as

$$\mathbf{Y} = \mathbf{HXQ} + \mathbf{Z}, \tag{1}$$

where $\mathbf{X} = [\mathbf{x}_1, \ldots, \mathbf{x}_M] \in \mathcal{F}^{N_{\mathrm{T}} \times M}$ is the transmit signal matrix employed for both radar and communication operations, M symbols is the length of the communication frame/radar pulse and $\mathcal{F}$ is the set of complex unit-modulus numbers, i.e.,

$$\mathcal{F} = \{\omega \in \mathbb{C} \mid |\omega| = 1\}. \tag{2}$$

For the case of finite resolution PS, the entries of the transmit signal $\mathbf{X}$ lie in set $\mathcal{F}_b \subset \mathcal{F}$ which is derived by the discretization of the complex unit circle, i.e.,

$$\mathcal{F}_b = \left\{1, e^{j\frac{2\pi}{2^{b+1}}}, \cdots, e^{j\frac{2\pi\left(2^{b+1}-1\right)}{2^{b+1}}}\right\}, \tag{3}$$

where b-bits resolution is assumed for all the involved PS modules. The channel matrix $\mathbf{H} = [\mathbf{h}_1, \ldots, \mathbf{h}_{N_{\mathrm{R}}}]^T \in \mathbb{C}^{N_{\mathrm{R}} \times N_{\mathrm{T}}}$

represents the frequency flat fading channel entries between the JRC system and the communication user terminals (UTs). The channel state information is assumed to be perfectly known at the transceiver. The matrix $\mathbf{Q} = \text{diag}([q_1, \ldots, q_M])$ is the $M \times M$ diagonal matrix of real entries that correspond to the common amplitude set by the VGA per frame of symbols.

The matrix $\mathbf{Z} = [\mathbf{z}_1, \ldots, \mathbf{z}_M] \in \mathbb{C}^{N_\text{R} \times M}$ represents the independent and identically distributed complex additive white Gaussian noise at the communication UTs where $\mathbf{z}_m \sim \mathcal{CN}(0, \sigma_\text{z}^2 \mathbf{I})$, $\forall m$ and σ_z^2 is the noise variance.

The communication part of the system aims at the transmission of a desired symbol $s(n,m) \in \mathcal{O}$, $1 \leq n \leq N_\text{R}$, $1 \leq m \leq M$, from the BS to the nth UT in the mth symbol time. $\mathcal{O}$ is the set of the employed constellation points with cardinality $|\mathcal{O}| = C$. In each symbol time, the vector of the symbols to be transmitted to the UTs is denoted by $\mathbf{s}_m \in \mathcal{O}^{N_\text{R} \times 1}$. Given the CSI and $\mathbf{S} = [\mathbf{s}_1, \ldots, \mathbf{s}_M]$, that includes the symbols to be transmitted to the N_R UTs at a block of M symbol times, the BS aims at the design of a transmit signal matrices, $\mathbf{X}$ and $\mathbf{Q}$ such that the matrix of the received signals at the UTs during these M symbol times $\mathbf{Y}$ is as close as possible, to $\mathbf{S}$.

The latter may be achieved by minimizing the so-called "MUI energy" [37], given by,

$$f(\mathbf{X}, \mathbf{Q}) = \|\mathbf{HXQ} - \mathbf{S}\|_F^2. \tag{4}$$

Observe that the received signal of the nth UT in the mth symbol time can be written as,

$$y_{n,m} = s_{n,m} + \underbrace{\mathbf{h}_n^T \mathbf{x}_m - s_{n,m}}_{\text{MUI at the } n\text{th user}} + z_{n,m}. \tag{5}$$

Then, according to (5), the receive SINR per block of M symbols for the nth UT, is defined as

$$\xi_n = \frac{\mathbb{E}\{|s_{n,m}|^2\}}{\mathbb{E}\{|\mathbf{h}_n^T \mathbf{x}_m - s_{n,m}|^2\} + N_0}, \tag{6}$$

where $s_{n,m}$ is the (n,m)th entry of the symbol matrix $\mathbf{S}$. In (6) the expectation operator in the numerator is applied on $s_{n,m}$ and in the denominator, it is applied on $s_{n,m}$ and $\mathbf{x}_m$, as well.

It has been shown in [37] that an approximation of the achievable normalized information rate for the nth user is a function of SINR term ξ_n, given in (6). Thus, the achievable sum-rate of the communication part can be approximated by,

$$r = \sum_{n=1}^{N_\text{R}} \log_2(1 + \xi_n), \tag{7}$$

where ξ_n is calculated by (6).

Let us assume that 1) the symbols $s_{m,n}$, where $1 \leq m \leq M$, $1 \leq n \leq N$, are drawn from the same constellation set $\mathcal{O}$ and have fixed energy. Then, the signal power $\mathbb{E}\{|s_{m,n}|^2\}$ in (6) is also fixed and thus, the SINR expression per user can be maximized by minimizing the MUI energy in (4). From (7), it is straightforward to see that by maximizing the SINR of the UTs, their achievable rate is maximized, as well. That is, the MUI energy minimization is a suitable criterion for optimizing the rate performance of the system.

In the proposed design, we aim at the optimization of the communication sum-rate of the JRC system through the minimization of the MUI energy subject to the constraints related to the radar waveform design and additionally due to the employed hardware, i.e., unit-modulus signals due to the PS and maximum transmission power constraints due to the VGA/PAs at the BS.

B. Radar Model

The transmit beampattern for the JRC system that points to the targets of interest can be expressed as

$$P_\text{T}(\theta) = \mathbf{a}_\text{T}^H(\theta) \mathbf{R}_\text{T} \mathbf{a}_\text{T}(\theta), \tag{8}$$

where $\mathbf{a}_\text{T}(\theta) = [1, e^{j\frac{2\pi}{\lambda} d \sin(\theta)}, ..., e^{j(N_\text{T}-1)\frac{2\pi}{\lambda} d \sin(\theta)}]^T$ is the transmit array response vector, with λ being the signal wavelength and d is the inter-element antenna spacing. The variable θ denotes the angle of detection. Note that the above expression represents the power of the transmitted signal at a general focal point θ as in [38]. The covariance matrix associated with the transmit signal matrix $\mathbf{XQ}$ is given by

$$\mathbf{R}_\text{T} = \frac{1}{M} \mathbf{XQQ}^H \mathbf{X}^H, \tag{9}$$

where it is assumed that $M \geq N_\text{T}$ without loss of generality, $\mathbf{R}_\text{T}$ in (9) is positive definite. Following [39], designing $\mathbf{R}_\text{T}$ is equivalent to designing the transmit radar beampattern in (8) for uncorrelated waveforms where MIMO radar exhibits high degree of freedom (DoF) in comparison to the conventional phased array radar. Having described the desired cost function and the desired features of the radar waveform, the optimization problem via which the transmit signals are derived for the low complexity analog architecture is defined in the next section.

III. Waveform Design

In this section, we formulate the waveform design problem and derive an algorithmic solution to solve the problem for the system model in Fig.1.

We consider $\mathbf{R}_\text{D}$ as a Hermitian positive semidefinite covariance matrix corresponding to a well-designed radar beampattern [10]. The transmit waveform design problem for the JRC system involves the derivation of the optimal $\mathbf{X}$ and $\mathbf{Q}$ matrices per block of M symbols through minimizing the MUI function in (4), that is

$$\begin{aligned} (\mathcal{P}_1): \quad & \min_{\mathbf{X},\mathbf{Q}} \frac{1}{2} \|\mathbf{S} - \mathbf{HXQ}\|_F^2 \\ & \text{s. t.} \quad \mathbf{X} \in \mathcal{F}^{N_\text{T} \times M}(\mathcal{F}_b^{N_\text{T} \times M}) \\ & \qquad \frac{1}{M} \mathbf{XQQ}^H \mathbf{X}^H = \mathbf{R}_\text{D} \\ & \qquad |\text{diag}\{\mathbf{Q}\}|^2 \preceq P_\text{max} \mathbf{1}, \end{aligned}$$

where the first constraint is due to the unit-modulus entries in $\mathbf{X}$, for the infinite and finite resolution PS cases, respectively, the second constraint imposes the desired beampattern to the transmit waveform and the third one is a maximum power budget related constraint (P_max).

Problem $(\mathcal{P}_1)$ is nonconvex due to the nonconvex objective function and nonconvex set of constraints. It is in general, a difficult NP-hard problem to solve [35]. In order to solve the directional beampattern design problem in $(\mathcal{P}_1)$, we can express it in a form solvable by an alternating minimization-based approach, called as primal-dual method (PDM) [36]. There are existing methods which implement alternating minimization based iterative procedures to solve constrained optimization problems efficiently. These methods provide a variant of the standard augmented Lagrangian method that uses partial updates (similar to the Gauss-Seidel method for the solution of linear equations) to solve optimization problems with constraints. This approach has been successfully applied to solve nonconvex problems, as well [40]- [42]. For convenience, we introduce the auxiliary matrix $\mathbf{Z}$, and problem $(\mathcal{P}_1)$ is rewritten as

$$\begin{aligned}(\mathcal{P}_2): \min_{\mathbf{Z},\mathbf{X},\mathbf{Q}} \frac{1}{2}\left\|\mathbf{S}-\mathbf{H}\mathbf{Z}\right\|_F^2 \\ \text{s. t. } \mathbf{Z}=\mathbf{X}\mathbf{Q} \\ \mathbf{X}\in\mathcal{F}^{N_{\mathrm{T}}\times M}(\mathcal{F}_b^{N_{\mathrm{T}}\times M}) \\ \frac{1}{M}\mathbf{Z}\mathbf{Z}^H=\mathbf{R}_{\mathrm{D}} \\ |\mathrm{diag}\{\mathbf{Q}\}|^2\preceq P_{\max}\mathbf{1}.\end{aligned}$$

Problem $\mathcal{P}_2$ is a nonconvex problem. However, the objective function is convex in Z. Furthermore, we have introduced an additional (first) constraint that captures the coupling between X and Q, and thus, there is no coupling term in the third constraint on the covariance matrix. The augmented Lagrangian function of the optimization problem $\mathcal{P}_2$ can be written as

$$\begin{aligned}\mathcal{L}_1(\mathbf{Z},\mathbf{X},\mathbf{Q},\mathbf{\Lambda}) =&\frac{1}{2}\left\|\mathbf{S}-\mathbf{H}\mathbf{Z}\right\|_F^2+\mathrm{tr}\big(\mathbf{\Lambda}^H(\mathbf{Z}-\mathbf{X}\mathbf{Q})\big)\\ &+\frac{\rho}{2}\left\|\mathbf{Z}-\mathbf{X}\mathbf{Q}\right\|_F^2,\end{aligned}\tag{10}$$

where $\rho\in\mathbb{R}_+$ is a scalar hyper-parameter and $\mathbf{\Lambda}\in\mathbb{C}^{N_{\mathrm{T}}\times M}$ is the Lagrange multiplier matrix having as entries the dual variables.

Then, the application of the proposed PDM for solving $\mathcal{P}_2$ involves the alternating minimization steps, with respect the primal variables, given by

$$\begin{aligned}(\mathcal{P}_{2A}):\ &\mathbf{Z}_{k+1}=\arg\min_{\mathbf{Z}\in\mathcal{Z}}\mathcal{L}_1(\mathbf{Z},\mathbf{X}_k,\mathbf{Q}_k,\mathbf{\Lambda}_k),\\ (\mathcal{P}_{2B}):\ &\mathbf{X}_{k+1}=\arg\min_{\mathbf{X}\in\mathcal{F}^{N_{\mathrm{T}}\times M}}\mathcal{L}_1(\mathbf{Z}_{k+1},\mathbf{X},\mathbf{Q}_k,\mathbf{\Lambda}_k),\\ (\mathcal{P}_{2C}):\ &\mathbf{Q}_{k+1}=\arg\min_{\mathbf{Q}\in\mathcal{Q}}\mathcal{L}_1(\mathbf{Z}_{k+1},\mathbf{X}_{k+1},\mathbf{Q},\mathbf{\Lambda}_k),\end{aligned}$$

where $\mathbf{Z}_k$, $\mathbf{X}_k$, $\mathbf{Q}_k$ and $\mathbf{\Lambda}_k$ are the variable values at the kth iteration of the PDM sequence and $\mathcal{Z}$ and $\mathcal{Q}$ are the sets associated with the constraints in $(\mathcal{P}_2)$. The dual variables in $\mathbf{\Lambda}_{k+1}$, $1\le m\le M$ are updated via a gradient ascent step, i.e.,

$$\mathbf{\Lambda}_{k+1}=\mathbf{\Lambda}_k+\gamma\left(\mathbf{Z}_{k+1}-\mathbf{X}_{k+1}\mathbf{Q}_{k+1}\right),\tag{11}$$

where $\gamma\in\mathbb{R}$ is a scalar step-size parameter. We now move forward with the derivation to the solution of $(\mathcal{P}_{2A})$, i.e.,

$$\begin{aligned}\min_{\mathbf{Z}} -\mathrm{tr}(\mathrm{re}(\mathbf{S}^H\mathbf{H}\mathbf{Z}))+\frac{1}{2}\|\mathbf{H}\mathbf{Z}\|_F^2+\mathrm{tr}(\mathrm{re}(\mathbf{\Lambda}_k^H\mathbf{Z}))\\ +\frac{\rho}{2}[\|\mathbf{Z}\|_F^2-2\mathrm{tr}(\mathrm{re}(\mathbf{Z}^H\mathbf{X}_k\mathbf{Q}_k))]\\ \text{subject to } \frac{1}{M}\mathbf{Z}\mathbf{Z}^H=\mathbf{R}_{\mathrm{D}}.\end{aligned}\tag{12}$$

We now utilize the constraint, $\mathbf{Z}\mathbf{Z}^H = M\mathbf{R}_D$ into the objective function. As a consequence, the second term of the objective function in the above problem becomes independent of $\mathbf{Z}$. Thus, after neglecting this constant-term, the simplified objective function can be written as, $-\mathrm{tr}(\mathrm{re}(\mathbf{Z}^H(\mathbf{H}^H\mathbf{S}-\mathbf{\Lambda}_k+\rho\mathbf{X}_k\mathbf{Q}_k)))$. After completing the square, the above problem can be further formulated as given by,

$$\begin{aligned}\min_{\mathbf{Z}} \quad &\left\|\mathbf{Z}-\hat{\mathbf{S}}\right\|_F^2\\ \text{subject to } &\frac{1}{M}\mathbf{Z}\mathbf{Z}^H=\mathbf{R}_{\mathrm{D}},\end{aligned}\tag{13}$$

where $\hat{\mathbf{S}}=\mathbf{H}^H\mathbf{S}-\mathbf{\Lambda}_k+\rho\mathbf{X}_k\mathbf{Q}_k$. The related constraint can be further expressed as,

$$\frac{1}{M}\mathbf{F}^{-H}\mathbf{Z}\mathbf{Z}^H\mathbf{F}^{-1}=\mathbf{I},$$

where $\mathbf{F}$ is calculated by the Cholesky decomposition of the covariance matrix $\mathbf{R}_{\mathrm{D}}$, i.e., $\mathbf{R}_{\mathrm{D}}=\mathbf{F}\mathbf{F}^H$, where the matrix $\mathbf{F}$ is a $N_{\mathrm{T}}\times N_{\mathrm{T}}$ lower triangular matrix. Matrix $\mathbf{F}$ is invertible since the covariance matrix $\mathbf{R}_{\mathrm{D}}$ is assumed to be positive definite. We let $\tilde{\mathbf{Z}}=\sqrt{\frac{1}{M}}\mathbf{F}^{-1}\mathbf{Z}$ and thus, we have

$$\begin{aligned}\min_{\mathbf{Z}} \quad &\left\|\sqrt{M}\mathbf{F}\tilde{\mathbf{Z}}-\hat{\mathbf{S}}\right\|_F^2\\ \text{subject to } &\tilde{\mathbf{Z}}\tilde{\mathbf{Z}}^H=\mathbf{I}.\end{aligned}\tag{14}$$

The above problem in (14) represents an orthogonal Procrustes problem (OPP) which admits the following closed-form solution:

$$\tilde{\mathbf{Z}}=\tilde{\mathbf{U}}\mathbf{I}_{N_{\mathrm{R}}\times M}\tilde{\mathbf{V}}^H,\tag{15}$$

where $\tilde{\mathbf{U}}\tilde{\mathbf{\Sigma}}\tilde{\mathbf{V}}^H=\mathbf{F}^H\hat{\mathbf{S}}$ represents the singular value decomposition (SVD) of $\mathbf{F}^H\hat{\mathbf{S}}$ where $\tilde{\mathbf{U}}$ and $\tilde{\mathbf{V}}$ are the left and right singular matrices of SVD, respectively, and $\tilde{\mathbf{\Sigma}}$ denotes the diagonal matrix of singular values. Thus, the update for variable $\mathbf{Z}$ is given by

$$\begin{aligned}\sqrt{\frac{1}{M}}\mathbf{F}^{-1}\mathbf{Z}_{k+1}&=\tilde{\mathbf{U}}\mathbf{I}_{N_{\mathrm{R}}\times M}\tilde{\mathbf{V}}^H\\ \implies \mathbf{Z}_{k+1}&=\sqrt{M}\mathbf{F}\tilde{\mathbf{U}}\mathbf{I}_{N_{\mathrm{R}}\times M}\tilde{\mathbf{V}}^H.\end{aligned}\tag{16}$$

We now derive the solution to $\mathcal{P}_{2B}$. We have,

$$\begin{aligned}\min_{\mathbf{X}} &-\mathrm{tr}(\mathrm{re}(\mathbf{\Lambda}_k^H\mathbf{X}\mathbf{Q}_k))\\ &+\frac{\rho}{2}[-2\mathrm{tr}(\mathrm{re}(\mathbf{Z}_{k+1}^H\mathbf{X}\mathbf{Q}_k))+\|\mathbf{X}_k\mathbf{Q}_k\|_F^2]\\ &\text{subject to } \mathbf{X}\in\mathcal{F}^{N_{\mathrm{T}}\times M}(\mathcal{F}_b^{N_{\mathrm{T}}\times M}),\end{aligned}\tag{17}$$

The solution to this problem does not admit a closed form and thus, we resort to a projected gradient descent approach for its solution [36]. That is, the update for variable $\mathbf{X}$ at the $(k+1)$th iteration is done through an iterative procedure that performs the following sequential updates on its $(l+1)$th iteration

$$\mathbf{X}_{k+1,l+1} = \Pi_{\mathcal{X}} \left\{ \mathbf{X}_{k+1,l} - \alpha \nabla_{\mathbf{X}} \mathcal{L}(\mathbf{Z}_{k+1}, \mathbf{X}_{k+1,l}, \mathbf{Q}_k, \mathbf{\Lambda}_k) \right\}, \tag{18}$$

where $\mathcal{X} = \mathcal{F}$ or $\mathcal{X} = \mathcal{F}_b$ and thus, $\Pi_{\mathcal{F}}\{\cdot\}$ and $\Pi_{\mathcal{F}_b}\{\cdot\}$ are the element-wise projection operators onto sets $\mathcal{F}$ and $\mathcal{F}_b$, respectively, $\mathbf{X}_{k+1,0} = \mathbf{X}_k$, α is a step-size parameter and the gradient $\nabla_{\mathbf{X}} \mathcal{L}(\mathbf{Z}, \mathbf{X}, \mathbf{Q}, \mathbf{\Lambda})$ is given by

$$\nabla_{\mathbf{X}} \mathcal{L}(\mathbf{Z}, \mathbf{X}, \mathbf{Q}, \mathbf{\Lambda}) = \mathbf{Q}\mathbf{\Lambda}^H - \rho[\mathbf{Q}\mathbf{Z}^H - \mathbf{Q}\mathbf{Q}^H\mathbf{X}^H]. \tag{19}$$

The projection operator $\Pi_{\mathcal{F}}\{\cdot\}$ can be computed by solving the following optimization problem,

$$\begin{aligned} (\mathcal{P}_3): \quad & \min_{\mathbf{A}_{\mathcal{F}}} \|\mathbf{A}_{\mathcal{F}} - \mathbf{A}\|_F^2 \\ & s.t.\ \mathbf{A}_{\mathcal{F}} \in \mathcal{F}^{N_{\mathrm{T}} \times M}, \end{aligned} \tag{20}$$

where $\mathbf{A}$ is an arbitrary matrix and $\mathbf{A}_{\mathcal{F}} = \Pi_{\mathcal{F}}\{\mathbf{A}\}$ is its element-wise projection onto the set $\mathcal{F}^{N_{\mathrm{T}} \times M}$. It can be shown that $(\mathcal{P}_3)$ admits the closed form solution given by

$$\mathbf{A}_{\mathcal{F}}(i_r, i_c) = \begin{cases} 0, & \mathbf{A}(i_r, i_c) = 0 \\ \frac{\mathbf{A}(i_r, i_c)}{|\mathbf{A}(i_r, i_c)|}, & \mathbf{A}(i_r, i_c) \neq 0 \end{cases}, \tag{21}$$

where $\mathbf{A}_{\mathcal{F}}(i_r, i_c)$ and $\mathbf{A}(i_r, i_c)$ are the elements at the i_rth row - i_cth column of matrices $\mathbf{A}_{\mathcal{F}}$ and $\mathbf{A}$, respectively and $1 \leq i_r \leq N_{\mathrm{T}}$ and $1 \leq i_c \leq M$.

In a similar manner, the projection operator onto the set $\mathcal{F}_b$ can be computed by solving the following optimization problem,

$$\begin{aligned} (\mathcal{P}_4): \quad & \min_{\mathbf{A}_{\mathcal{F}_b}} \|\mathbf{A}_{\mathcal{F}_b} - \mathbf{A}\|_F^2 \\ & s.t.\ \mathbf{A}_{\mathcal{F}_b} \in \mathcal{F}_b^{N_{\mathrm{T}} \times M}, \end{aligned} \tag{22}$$

where $\mathbf{A}$ is again, an arbitrary matrix, and $\mathbf{A}_{\mathcal{F}_b} = \Pi_{\mathcal{F}_b}\{\mathbf{A}_b\}$ is its element-wise projection onto the set $\mathcal{F}_b^{N_{\mathrm{T}} \times M}$. It can be shown that problem $\mathcal{P}_4$ admits the following element-wise solution,

$$\mathbf{A}_{\mathcal{F}_b}(i_r, i_c) = \arg \min_{0 \leq i \leq 2^b} \left| \mathbf{A}(i_r, i_c) - e^{j\frac{2\pi i}{2^{b+1}}} \right|^2, \tag{23}$$

where $\mathbf{A}_{\mathcal{F}_b}(i_r, i_c)$ and $\mathbf{A}(i_r, i_c)$ are the elements at the i_rth row - i_cth column of matrices $\mathbf{A}_{\mathcal{F}_b}$ and $\mathbf{A}$, respectively, and again, $1 \leq i_r \leq N_{\mathrm{T}}$ and $1 \leq i_c \leq M$. In other words, $\mathbf{A}(i_r, i_c)$ is quantized to the closest value in $\mathcal{F}_b$.

Ideally, the iterations in (18) should run until a termination criterion is met, i.e., such that convergence to an optimal point of $\mathcal{P}_{2B}$ is established. In order to reduce the required complexity, we propose to run the inner iteration (index l) in (18) only for a few iterations (L_{max}) for every outer iteration (index k), thus resulting in an inexact solution for updating the variable $\mathbf{X}$. In the recent literature, PDM-based solutions with inexact updates have been successfully applied to solve optimization problems [43], [44]. This can be further explained by theoretical results showing that under certain conditions, PDM with alternating minimization steps that are not exactly carried out are possible to converge [36], [44], [45]. Nevertheless, a detailed theoretical study is beyond the scope of the present work. The derived inexact solution appears to behave remarkably well, as it is verified by the numerical results in Sec. V.

Next, we derive the solution to $\mathcal{P}_{2C}$,

$$\begin{aligned} \min_{\mathbf{Q}} & -\mathrm{tr}(\mathrm{re}(\mathbf{\Lambda}^H\mathbf{X}\mathbf{Q})) + \frac{\rho}{2}[-2\mathrm{tr}(\mathrm{re}(\mathbf{Z}^H\mathbf{X}\mathbf{Q})) + \|\mathbf{X}\mathbf{Q}\|_F^2] \\ & \text{subject to } |\mathrm{diag}\{\mathbf{Q}\}|^2 \preceq P_{\max}\mathbf{1}. \end{aligned} \tag{24}$$

Problem $\mathcal{P}_{2C}$ is a convex optimization problem, however, it does not admits a closed-form solution. Thus, we resort once more to a projected gradient descent approach for its solution with the update at the $(l+1)$th iteration given by,

$$\mathbf{Q}_{k+1,l+1} = \Pi_{\mathcal{Q}} \left\{ \mathbf{Q}_{k+1,l} - \mu' \nabla_{\mathbf{Q}} \mathcal{L}(\mathbf{Z}_{k+1}, \mathbf{X}_{k+1}, \mathbf{Q}_k, \mathbf{\Lambda}_k) \right\}, \tag{25}$$

where $\mathbf{Q}_{k+1,0} = \mathbf{Q}_k$, μ' is a step-size parameter, the gradient $\nabla_{\mathbf{Q}} \mathcal{L}(\mathbf{Z}, \mathbf{X}, \mathbf{Q}, \mathbf{\Lambda})$ is given by

$$\nabla_{\mathbf{Q}} \mathcal{L}(\mathbf{Z}, \mathbf{X}, \mathbf{Q}, \mathbf{\Lambda}) = \mathbf{\Lambda}^H\mathbf{X} - \rho\left(\mathbf{Z}^H\mathbf{X} - \mathbf{Q}^H\mathbf{X}^H\mathbf{X}\right), \tag{26}$$

and the projection operator $\Pi_{\mathcal{Q}}$ can be derived by solving the following optimization problem,

$$\begin{aligned} (\mathcal{P}_5): \quad & \min_{\mathbf{A}_{\mathcal{Q}}} \|\mathbf{A}_{\mathcal{Q}} - \mathbf{A}\|_F^2 \\ & s.t.\ \mathbf{A}_{\mathcal{Q}} \in \mathcal{Q}, \end{aligned} \tag{27}$$

where $\mathbf{A}$ is again, an arbitrary matrix and $\mathbf{A}_{\mathcal{Q}}$ is its element-wise projection of the onto the set $\mathcal{Q}$. It can be shown that $(\mathcal{P}_5)$ admits the closed form solution given by

$$\mathbf{A}_{\mathcal{Q}}(i,j) = \begin{cases} \mathbf{A}(i,j), & i = j \ \&\ |\mathbf{A}(i,j)|^2 \leq P_{\max}, \\ \sqrt{P_{\max}}\frac{\mathbf{A}(i,i)}{|\mathbf{A}(i,i)|}, & i = j \ \&\ |\mathbf{A}(i,i)|^2 > P_{\max} \\ 0, & i \neq j, \end{cases} \tag{28}$$

where $\mathbf{A}_{\mathcal{Q}}(i,j)$ and $\mathbf{A}(i,j)$ are the (i,j)th elements of matrices $\mathbf{A}_{\mathcal{Q}}$ and $\mathbf{A}$, respectively. Following the discussion for the solution to $\mathcal{P}_{2B}$, we also here opt for an inexact solution for the inner iteration updates in (25) which are performed for again L_{max} iterations.

The alternating optimization procedure via which the values of $\mathbf{Z}, \mathbf{X}, \mathbf{Q}$ and $\mathbf{\Lambda}$ are derived runs in an iterative manner until convergence is achieved. We propose termination criteria for the alternating minimization procedure, as given by,

$$\|\mathbf{Z}_{k+1} - \mathbf{Z}_k\|_F \leq \epsilon_z \ \& \tag{29}$$

$$\|\mathbf{Z}_{k+1} - \mathbf{X}_{k+1}\mathbf{Q}_{k+1}\|_F \leq \epsilon_p, \tag{30}$$

where ϵ_z and ϵ_p are the corresponding tolerances. The first termination criterion guarantees the convergence of variable $\mathbf{Z}_k$ and further the convergence of $(\mathcal{P}_{2A})$. The second one guarantees that the primal feasibility condition of $(\mathcal{P}_2)$ is satisfied. Due to the nonconvex nature of the latter problem, it is also useful to add a termination criterion related to the maximum permitted number of iterations of the PDM sequence, defined as K_{max}. The complete procedure is summarized in Algorithm 1. The computational complexity per iteration is $O(M^3)$ due to the SVD calculation in the solution of $\mathcal{P}_{2A}$ and under the reasonable assumption that in general $M > N_{\mathrm{T}}$.

We may now comment on the convergence properties of the proposed approach. In the literature so far, strong convergence results for PDM-based solutions have been derived for convex

Algorithm 1 Proposed Method for JRC system's Waveform Design

Initialize: $\mathbf{X}_0 \in \mathcal{F}^{N_{\mathrm{T}}\times M}$, $\mathbf{Z}_0$ to be matrix satisfying $\frac{1}{M}\mathbf{Z}_0\mathbf{Z}_0^H = \mathbf{R}_{\mathrm{D}}$ and initialize $\mathbf{\Lambda}_0$ with zeros
while The criteria in (29)-(30) are not satisfied or $k \leq K_{max}$ **do**
  $k \leftarrow k+1$
  Calculate $\hat{\mathbf{S}} = (\mathbf{H} + \mathbf{G}_2\mathbf{\Omega}\mathbf{G}_1)^H\mathbf{S} - \mathbf{\Lambda}_k + \rho\mathbf{X}_k\mathbf{Q}_k$
  Compute the SVD of $\mathbf{F}^H\hat{\mathbf{S}}$ and calculate $\tilde{\mathbf{Z}}$ by (15)
  Update $\mathbf{Z}_{k+1}$ using solution (16)
  $\mathbf{X}_{k+1,0} \leftarrow \mathbf{X}_k$, $l \leftarrow 1$
  for $l \leq L_{max}$ **do**
    $l \leftarrow l+1$
    Update $\mathbf{X}_{k+1,l+1}$ using solution (18) by using the projection (21) and (23) for the infinite and finite resolution PS cases, respectively.
  end for
  $\mathbf{X}_{k+1} \leftarrow \mathbf{X}_{k+1,L_{max}}$
  $\mathbf{Q}_{k+1,0} \leftarrow \mathbf{Q}_k$, $l \leftarrow 1$
  for $l \leq L_{max}$ **do**
    $l \leftarrow l+1$
    Update $\mathbf{Q}_{k+1}$ using solution (25)
  end for
  $\mathbf{Q}_{k+1} \leftarrow \mathbf{Q}_{k+1,L_{max}}$
  Update $\mathbf{\Lambda}_{k+1}$ using (11)
end while
return $\mathbf{X}_\star$,$\mathbf{Q}_\star$

problems having two blocks of variables [46]. Furthermore, for nonconvex problems, strong convergence guarantees are in general unknown and also an open research problem. Problem $(\mathcal{P}_2)$ involves three blocks of variables and it involves a nonconvex objective function and feasible solution set. Therefore, the derivation of strong convergence results is an intractable task and beyond the scopes of the present work.

IV. Power Consumption Model

In this section, we derive the model for the transceiver's power consumption based on the employed architecture shown in Fig. 1a. The derived power consumption is used later in Sec. V to plot the energy efficiency of the examined systems.

Let us first derive an approximate power consumption model for the single antenna system of each fully digital receiver. Following the results in [47], one may show that the consumed power at each one of the receivers can be approximately modeled by,

$$P_{cr}(B', f_s) \approx P_{LNA} + 2P_{ADC}(B', f_s) + P_{RF} + P_{LO}, \quad (31)$$

where P_{LNA} is the power consumed by the Low Noise Amplifiers (LNAs), P_{RF} is the power consumed by the analog components of the RF chain, i.e. filters and mixers, P_{LO} is the power consumed at the local oscillator and $P_{ADC}(B', f_s)$ is the power consumed by a B'-bit ADC functioning with sampling frequency f_s with power consumption given by [47],

$$P_{ADC}(B', f_s) \approx \frac{3V_{dd}^2 L_{min} f_s}{2\times 10^{\frac{6.02B'+1.76}{10}}}, \quad (32)$$

where V_{dd} is the power supply, L_{min} is the minimum channel length for the employed Complementary Metal Oxide Semiconductor (CMOS) technology, the sampling frequency f_s, may be approximated as $f_s = 2(2f_b + f_{cor})$, where f_b is the employed bandwidth and f_{cor} is the corner frequency of the $1/f$ noise [47]. We may now move to the derivation of the power consumption of the analog transmitter's architecture in Fig. 1a. Based on the proposed architecture, the power consumption at the transmitter's side (BS) is given by,

$$P_{ct}^A(N_{\mathrm{T}}) \approx \frac{\mathbb{E}\{\|\mathbf{x}\|_2^2\}}{\eta} + P_{VGA} + P_{LO} + N_{\mathrm{T}}(P_{PS} + P_{RF}), \quad (33)$$

where η is the efficiency of the PAs, P_{VGA} and P_{PS} is the power consumption of the VGA and the PS, respectively. From (31) and (33), the total power consumption for the analog architecture in Fig. 1a is given by

$$P_c^A(B', f_s, N_{\mathrm{T}}, N_{\mathrm{R}}) = P_{ct}^A(N_{\mathrm{T}}) + N_{\mathrm{R}}P_{cr}(B', f_s). \quad (34)$$

Finally, let us calculate the power consumption of a system based on a fully digital BS (Fig. 1b) and the fully digital single antenna receivers whose performance will be examined in Sec. V for comparison purposes. An approximate model for the power consumption of a fully digital BS is given by [47],

$$P_{ct}^{FD}(N_{\mathrm{T}}, B, f_s) \approx \frac{\mathbb{E}\{\|\mathbf{x}\|_2^2\}}{\eta} + N_{\mathrm{T}}[2P_{DAC}(B, f_s) + P_{RF}] + P_{LO}, \quad (35)$$

where $P_{DAC}(B, f_s)$ is the power consumed by a B-bit DAC functioning with sampling frequency f_s.

We now provide the model for the power consumption of the DAC. According to the analysis in [47], the previous is approximated by

$$P_{DAC}(B, f_s) \approx \frac{\alpha_d}{2}\left[V_{dd}I_0(2^B - 1) + C_p f_s V_{dd}^2 B\right], \quad (36)$$

where V_{dd} is the power supply, I_0 is the unit current source that corresponds to the least significant bit, C_p is the parasitic capacitance of the switches used to select the DACs' supported states and α is a correcting factor that may be used to introduce some second order effects to the model.

It is now straightforward to see that the total power consumption of a system of N_{T} antennas fully digital BS and N_{R} users is given by,

$$P_c^{FD}(B, B', f_s, N_{\mathrm{T}}, N) = P_{ct}^{FD}(N_{\mathrm{T}}, B, f_s) + N_{\mathrm{R}}P_{cr}(B', f_s). \quad (37)$$

In the next section, the performance of the proposed JRC system is evaluated under different regimes.

V. Numerical Results

We evaluate the performance of the proposed JRC system designs for a BS with $N_{\mathrm{T}} = 16$ transmit antennas serving $N_{\mathrm{R}} = 6$ users. The communication frame/radar pulse length is set to $M = 30$ symbols and maximum transmit power equals to $P_{\max} = 1$ W. We assume an ULA-based setup where antenna elements are spaced by half-wavelength distance, i.e., $d = \lambda/2$ where λ can be based on a standard frequency value [10]. We set the number of targets to be three and

the corresponding angular target locations at $[-\pi/3, 0, \pi/3]$. The desired $\mathbf{R}_{\mathrm{D}}$ matrix variable is obtained by a least-squares approach such as in [39]. The entries of symbol matrix $\mathbf{S}$ is drawn from a quardature phase shift keying (QPSK) constellation. The signal-to-noise ratio (SNR) is defined as $1/\sigma_z^2$ and channel matrix $\mathbf{H}$ has complex Gaussian elements of zero mean and variance equal to 1, i.e. $\mathcal{CN}(0,1)$. One-bit resolution PS are considered for the finite resolution case. The hyper-parameter in (10) and step sizes for the gradient descent steps in (18) and (25), and the gradient ascent step (11) are set to $\rho = 10^2$, $\alpha = 10^{-2}$ and $\mu = 10^{-2}$, and $\gamma = 10^{-2}$, respectively, for the infinite and the finite resolution PS cases. The inner updates of the gradient descent steps are performed for $L_{max} = 10$ iterations. The tolerance variables in the termination criteria in (29)-(30) are set to $\epsilon_z = 10^{-4}$ and $\epsilon_p = 10^{-2}$, respectively. The maximum number of outer iterations is set to $N_{max} = 100$. The results are averaged over 10000 channel realizations. Note that this is the core simulation setup, though in several cases we differentiate from this model in order to gain insight to the impact of the system model's parameters on its performance. In such cases, we will explicitly present the differences from the core setup.

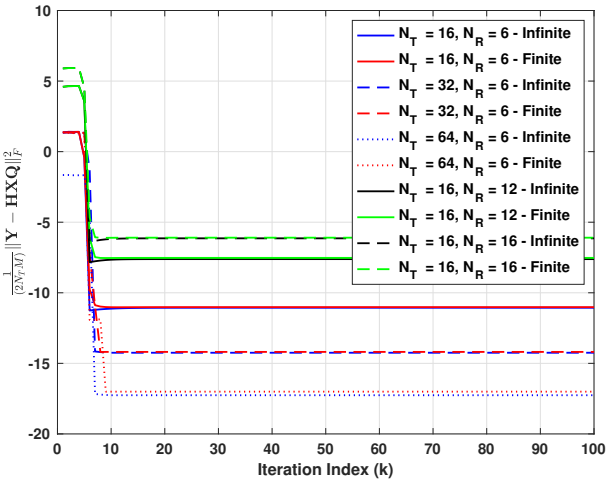

Fig. 2: Convergence study of Algorithm 1 for different system model parameters.

We compare the proposed designs with the following fully-digital baselines:

1) The state-of-the-art *directional-strict* approach which aims to design the radar beampattern with strict equality constraints. A detailed description of this approach can be found in [10].
2) The *directional trade-off* design which allows a tolerable mismatch between the desired radar beampattern and the designed one in order to form a balance with the communication performance [11]. The value of the weighting factor for communication and radar operations in trade-off case is chosen as 0.5.
3) The *zero MUI* case represents the performance lower bound for MUI and achieves the maximum rate performance [11].

Fig. 2 shows the convergence behaviour of Algorithm 1 for both the cases of infinite and finite resolution PS. In this figure, we plot the evolution of the normalized objective function in $(\mathcal{P}_1)$ per the outer iteration index k. It can be observed that in both the aforementioned cases, Algorithm 1 rapidly converges to a fixed point for the given numerical parametric values. Note that for the finite resolution case, Algorithm 1 appears to have slightly slower convergence compared to the infinite resolution one. This is the case, since the finite resolution problem involves the simultaneous optimization of discrete and continuous complex variables and thus it is, in general, more difficult to address than the one based on the infinite resolution PS. It can also be seen that for a phase shifting network employing PSs with only one-bit resolution, Algorithm 1 converges to the objective function value very close to the case when an infinite resolution phase shifting network is used. This explains the excellent performance of the JRC system for the one-bit PS cases, shown in the figures below. In the same figure, we also examine the impact of the number of transmitter's antennas N_T on the convergence of Algorithm 1. To that end, we plot the convergence performance for $N_T = 32$ and $N_T = 64$ while the values of the rest parameters remains fixed to the ones of the core setup. As can be seen for both the infinite and finite resolution PSs cases, as the number of transmitter's antennas increases, Algorithm 1 is able to converge to a lower objective value which is expected due to the increase on the available spatial degrees of freedom that can be used to suppress the interference and construct effectively the symbols to be transmitted to the communication UTs over the wireless channel. In addition, in Fig. 2 we also plot the performance of the core system setup that now serves $N_R = 12$ and $N_R = 16$ users. As the number of users increases, Algorithm 1 converges to higher objective value for both the infinite and finite resolution PSs cases which is a direct consequence of the fact that now more users have to be served while the number of spatial degrees of freedom remains the same, hence the increase in the MUI term. Apart from these observations, both the increase in the number of antennas and users do not change the behavior of Algorithm which still rapidly converges to close objective values for both the infinite and the finite resolution PSs.

Fig. 3 shows the average achievable sum-rate performance described in (7) with respect to (w.r.t.) the transmit Signal-to-Noise Ratio (SNR), defined as

$$\zeta = \frac{\mathbb{E}\{\|q_m \mathbf{x}_m\|_2^2\}}{\sigma_z^2}, \; 1 \leq m \leq M. \tag{38}$$

At first, it can be observed that the proposed PDM achieves better rate performance than the state-of-the-art directional-strict approach. This is the case, since in the proposed approach a relaxed version of the original problem is treated via the optimization of the augmented Lagrangian. That is, the desired beampattern is imposed in a sense that $\|\mathbf{Z}-\mathbf{XQ}\|_F \rightarrow 0$. In general, for small ρ values more weight is given to the MUI term compared to the beampattern imposing term. This explains the observed better performance of the proposed approach compared to the one of the directional-strict solution that imposes the exact beampattern to the desired signals. For example, at $\zeta = 10$ dB SNR, the proposed method

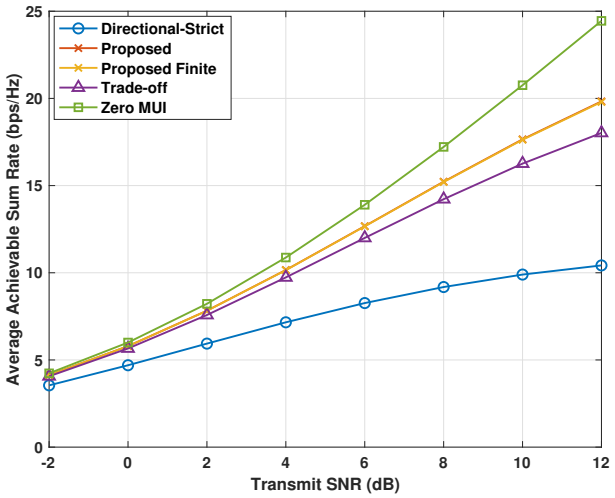

Fig. 3: Sum rate vs transmit SNR performance comparison for different methods with $N_{\mathrm{T}}=16$, $N_{\mathrm{R}}=6$ and $M=30$.

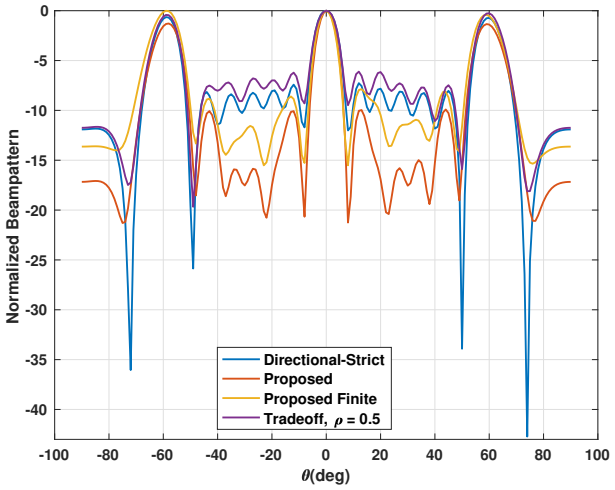

Fig. 4: Radar beampattern performance for different methods with $N_{\mathrm{T}}=16$, $N_{\mathrm{R}}=6$ and $M=30$.

outperforms the directional-strict case by $\approx$ 5 bits/s/Hz. Furthermore, the proposed PDM also outperforms the trade-off method and the performance in comparison with the zero MUI case is also satisfactory given the simplicity of the hardware architecture that implements the proposed approach. Moreover, the system with the one-bit PS achieves almost identical sum-rate with the one of the infinite resolution PS, as it was expected based on the convergence results, shown in Fig. 2.

Fig. 4 shows the radar beampattern performance plot for the proposed PDM and the baselines. It can be seen that the proposed PDM exhibits favourable transmit beampattern performance close to the one of directional-strict baseline at different target locations for both the infinite and the finite resolution phase shifting network cases. In the beampattern plot, the three major lobes for three targets can be observed at the angle locations of $[-\pi/3, 0, \pi/3]$.

In order to provide further insights on the radar parts' performance, the target detection probability for the considered setup in Fig. 4 is presented in Table I for radar noise variance equal to $\sigma_u^2 = \{0.01, 0.1, 1\}$. Furthermore, the detection probability for the cases of $N_T = 32$ and $N_T = 64$ transmit antennas is shown, as well. The detection probability is derived assuming that the radar system implements a target detector following the Neyman-Pearson approach [48]. The radar receiver formulates a binary hypothesis test, following the classical detection theory methodology, i.e.,

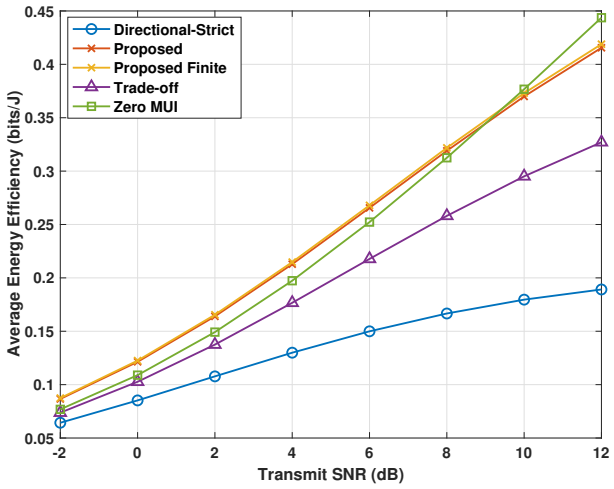

Fig. 5: Energy efficiency vs transmit SNR performance comparison for different methods with $N_{\mathrm{T}}=16$, $N_{\mathrm{R}}=6$ and $M=30$.

$$\mathcal{H}_0 : \text{No target exists}$$
$$\mathcal{H}_1 : \text{At least one target exist.}$$

Under $\mathcal{H}_0$, none of the targets of interest are present and the radar receiver signal is constituted by the clutter and noise components only. Under $\mathcal{H}_1$, at least one of the targets of interest is present and the radar receiver signal includes the signal generated by the reflections on the target(s) on top of the clutter and noise components. The radar receiver feeds the received signals to a detector which determines whether $\mathcal{H}_0$ or $\mathcal{H}_1$ holds. According to the Neyman-Pearson approach, this radar detector is designed such that the detection probability is maximized subject to a constraint that sets the false alarm probability above a predefined level P_{fa}.

According to the Neyman-Pearson approach, this radar detector is designed such that the detection probability is minimized subject to a constraint that sets the false alarm probability above a predefined level. By following the Neyman-Pearson methodology [48], it can be shown that the detection probability is minimized by comparing the radar's receive signal energy with a threshold δ: If the sufficient statistic is below that threshold, we conclude that no target is present ($\mathcal{H}_0$ holds). Otherwise, we conclude that at least one target is present ($\mathcal{H}_1$ holds).

The threshold is determined by equating the false alarm probability with the desired threshold since it can be shown that this strategy achieves the optimum detection performance [48]. Now, observe that a false alarm event emerges when the sufficient test statistic is above the threshold δ while

hypothesis $\mathcal{H}_0$ holds. To avoid unnecessary repetition, we omit the details of the derivation of the target detection probability. For more information, the interested reader can check [48].

By inspecting Table I, the good detection performance of the proposed approach is verified for both the infinite and the 1-bit resolution PSs cases as compared to the baseline approaches (Directional-Strict and Trade-off). Furthermore, as the number of antennas increases, the performance improves (wherever there is space for improvements) due to the additional available degrees of freedom that are able to effectively support the joint communication-radar functionality.

In Table II, we examine the impact of the number of communication UTs to the target detection probability. To that end, a JRC system with $N_T = 16$ transmit antennas is considered serving $N_R = \{6, 12, 16\}$ UTs. The remaining parameters are set based on the core setup. At first let us observe that the Directional-Strict one present degradation on the performance with an increase in the number of served users due to the subsequent increase on the MUI for the same spatial degrees of freedom. The Directional-Strict one focuses on the accurate beampattern design at the cost of significantly degrading the performance of the communication system, hence the observed good target detection performance. For the infinite resolution case, the proposed approach is able to achieve also flawless detection performance with a small degradation on the communication part's performance as the number of supported users increases, as it is shown later in Fig. 6. Furthermore, it is noteworthy to point out that the observed performance degradation is very small for the infinite resolution case. That is, the 1-bit case presents always less than 10% performance degradation, even for relative high radar noise variance values which is acceptable considering that the employed PSs support only two states. As shown latter in Table IV, the radar performance of the JRC system can benefit from an increase in resolution bits of the PSs.

In order to provide further insights on the performance, we examine the energy efficiency of the different techniques defined as the ratio of achievable sum-rate in (7) to the power consumption of the corresponding system as calculated in Section IV. The parameters used for calculating the power consumption of the different transceivers are shown in Table III. The achieved energy efficiency versus the transmit SNR (38) is shown in Fig. 5 for each one of the examined cases. Both the PDM based approaches achieve significantly increased energy efficiency compared to the existing "Directional-Strict" and "Trade-off" approaches since the latter exhibit higher power consumption due to the fully digital transmitter. That is, in the latter case, the BS presents much higher complexity and power consumption due to the $2N_{\mathrm{T}}$ DAC components required for its implementation (35). Furthermore, the 1-bit PS case appears to have slightly improved performance compared to the infinite resolution PS case. This is due to the lower power consumption as the resolution bits decrease and given their comparable performance with respect to the achieved sum-rate metric.

We continue our study on the performance of the new JRC transceiver design by examining the impact of the users' number on the systems performance. All of the parameters

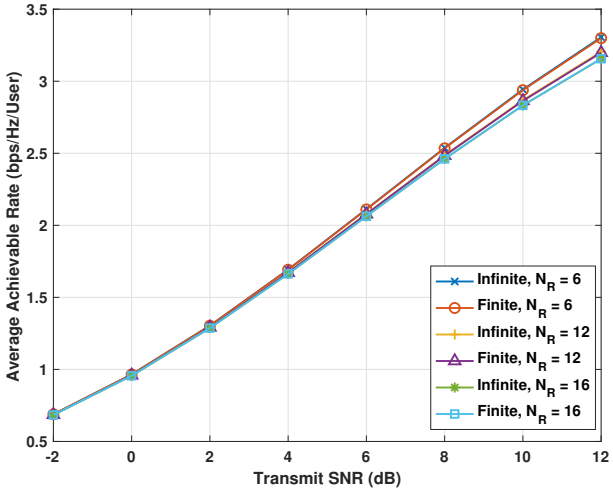

Fig. 6: Impact of the number of users to the average rate per user for $N_{\mathrm{T}}=16$, $N_{\mathrm{R}}=6, 12, 16$ and $M = 30$.

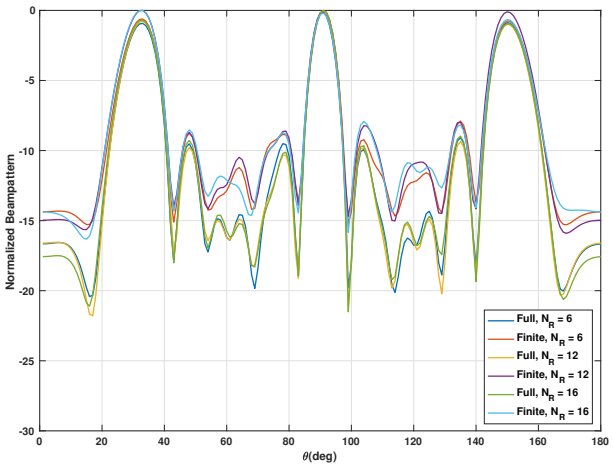

Fig. 7: Impact of the number of users to the Radar beampattern performance for different methods with $N_{\mathrm{T}}=16$, $N_{\mathrm{R}}=6, 12, 16$ and $M = 30$.

are set to the same values as in the experiments in Figs. 2-5, though now we consider the cases of $N_{\mathrm{R}} = 6, 12, 16$ users. The average achieved rate per user with respect the transmit SNR and the beampattern for both the systems with 1-bit and infinite resolution PS are shown in Fig. 6 and Fig. 7, respectively. As can be seen from both figures, the system achieves highly satisfactory performance for both the communication and radar functionality. Moreover, the average achievable rate performance slightly degrades as the number of served communication users increases. This is reasonable given that more number of users have to be served through the same spatial degrees of freedom, i.e., number of BS antennas.

Therefore, adding more users to the system will inevitably result in increased MUI per user and as a consequence reduction to their SINR/rate (4)-(7).

The impact of the block of processed symbols M on the performance of the JRC system is studied in Figs. 8-9. There, the achieved sum-rate versus the transmit SNR and the beampattern is plotted for the systems with 1-bit and

TABLE I: Radar Target Detection Probability vs Number of Transmit Antennas N_T

	P_d ($N_T = 16$)			P_d ($N_T = 32$)			P_d ($N_T = 64$)		
σ_u^2	0.01	0.1	1	0.01	0.1	1	0.01	0.1	1
Directional-Strict	1.000	1.000	1.000	1.000	1.000	1.000	1.000	1.000	1.000
Proposed	1.000	1.000	1.000	1.000	1.000	1.000	1.000	1.000	1.000
Proposed Finite	0.999	0.998	0.981	1.000	1.000	0.996	1.000	1.000	1.000
Trade-off	1.000	1.000	1.000	1.000	1.000	1.000	1.000	1.000	1.000

TABLE II: Radar Target Detection Probability vs Number of UTs N_R

	P_d ($N_R = 6$)			P_d ($N_R = 12$)			P_d ($N_R = 16$)		
σ_u^2	0.01	0.1	1	0.01	0.1	1	0.01	0.1	1
Directional-Strict	1.000	1.000	1.000	1.000	1.000	1.000	1.000	1.000	1.000
Proposed	1.000	1.000	1.000	1.000	1.000	1.000	1.000	1.000	1.000
Proposed Finite	0.999	0.998	0.981	0.992	0.978	0.935	0.982	0.978	0.915
Trade-off	1.000	1.000	1.000	0.686	0.686	0.684	0.682	0.682	0.680

TABLE III: Parameters for Energy Efficiency Calculation

N_{T}	16
N_{R}	6
M	30
η	0.35
P_{max}	1
P_{RF}	32.8mW
P_{LO}	50mW
P_{LNA}	20mW
P_{VGA}	9.5mW
B	14-bits
B'	14-bits
α_d	1
V_{dd}	3V
I_0	10μA
C_p	1pF
f_b	10KHz
f_{cor}	1MHz
L_{min}	0.5μm
$P_{PS}(\infty$-bits)	30mw
P_{PS}(1-bit)	3mw

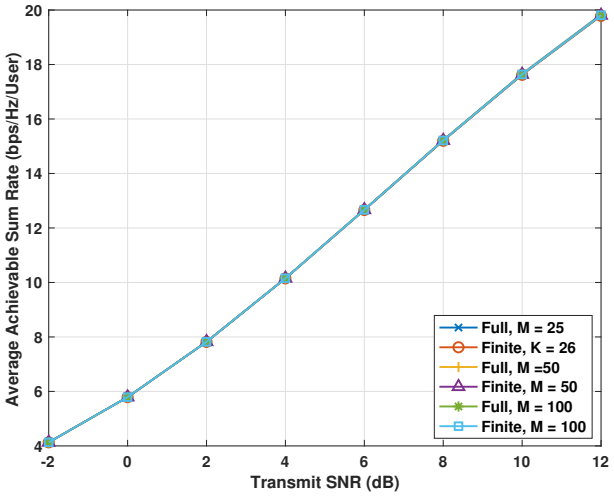

Fig. 8: Impact of M to the sum-rate for $N_{\mathrm{T}}=16$, $N_{\mathrm{R}}=6$ and $M = 25, 50, 100$.

infinite resolution PS, respectively. The followed simulation setup is similar with the ones of Figs. 2-5, though now the block of processed symbols length is set to $M = 25, 50, 100$. As observed, the PDM is able to design the transmit signals equally well for the different number of block of processed symbols hence, the comparable performance for both the communication and the radar functionality of the JRC system. Thus, we can conclude that the block size M has negligible impact on the system performance.

In Fig. 10, the impact of the number of transmit antennas N_T on the average achievable sum-rate of the proposed approaches is shown versus the transmit SNR (dB). The core simulation setup is considered for $N_{\mathrm{T}} = \{16, 32, 64\}$. As expected from the results in Fig. 2, the proposed approaches benefit from the available degrees of freedom and are able to improve their performance as the number of transmit antenna increases.

Finally, we compare the performance of the JRC system under different resolutions for the employed PSs. To that end, in Fig. 11, we plot the sum rate performance of the communication part under different resolutions for the PSs. Furthermore, in Table IV, the target detection probability is presented under different resolutions. Both the results in Fig. 11 and Table IV are generated based on the core simulation setup. As can been seen, the performance is almost identical for the communication part under any resolution. This is in line with the results shown in Fig. 2 where the proposed approach converged to the same the objective function value for both the infinite and 1-bit resolution case. That is, the 1-bit case is able to achieve the minimum MUI value for the communication part even with one bit resolution. On the contrary, there is space for improving performance, since as the resolution increases, the detection performance also improves. For the considered setup, a 3-bit resolution suffices to achieve both excellent communication performance and flawless radar one.

VI. Conclusion

This paper proposes a low complexity analog architecture to design an efficient MIMO JRC system via a phase shifting network and a VGA component. The cases of infinite resolution and finite resolution phase shifting networks are considered. Then, the transmit waveform of the proposed JRC

TABLE IV: Radar Target Detection Probability vs PSs Resolution

	P_d		
σ_u^2	0.01	0.1	1
Infinite	1.000	1.000	0.992
1-bit	0.999	0.998	0.981
2-bit	1.000	1.000	0.998
3-bit	1.000	1.000	1.000
4-bit	1.000	1.000	1.000

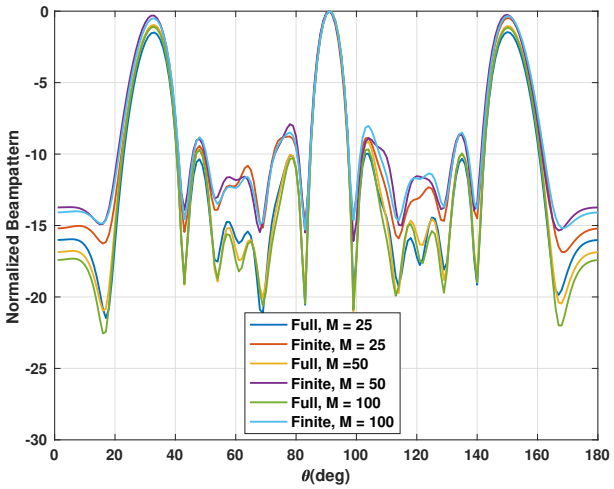

Fig. 9: Impact of M to the Radar beampattern performance for different methods with $N_{\mathrm{T}}=16$, $N_{\mathrm{R}}=6$ and $M=25,50,100$.

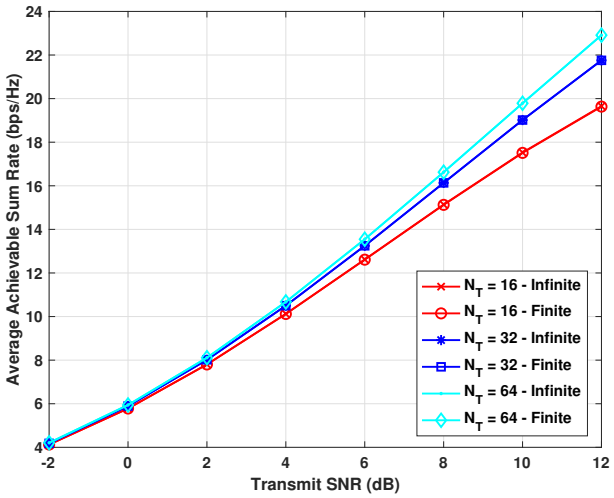

Fig. 10: Sum rate vs transmit SNR performance comparison for the proposed methods with $N_{\mathrm{T}}=\{16,32,64\}$, $N_{\mathrm{R}}=6$ and $M=30$.

system is obtained via the formulation of a downlink MUI minimization problem with architecture specific constraints and corresponding to the desired radar beampattern. An efficient solution based on the primal-dual framework is proposed to solve the nonconvex NP-hard optimization problem that achieves fast convergence. The proposed approach achieves high spectral efficiency and energy efficiency gains when compared with the state-of-the-art fully digital methods that

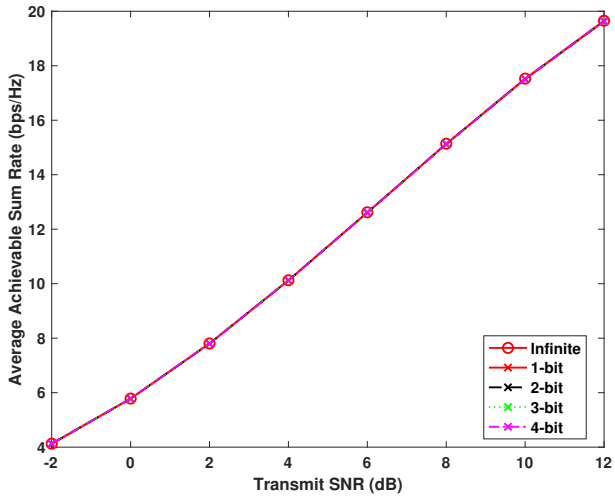

Fig. 11: Sum rate vs transmit SNR performance comparison under different PSs resolutions. A system with $N_{\mathrm{T}}=16$, $N_{\mathrm{R}}=6$ and $M=30$ is considered.

exhibit high implementation and power consumption costs. A desirable radar beampattern performance is also observed which infers the proposed approach to be an efficient solution for both communication and radar operations. Furthermore, as verified by the results, even 1-bit resolution PS suffices to achieve satisfactory performance for both the radar and the communication parts of the JRC system. Future works include the development of low complexity analog architectures for wide-band JRC systems and under the assumption of imperfect CSI knowledge.

REFERENCES

[1] Cisco, "Cisco - public cisco annual internet report, 2018–2023," *White Paper*, vol. 1, 2018.

[2] J. Lin, W. Yu, N. Zhang, X. Yang, H. Zhang, and W. Zhao, "A survey on internet of things: Architecture, enabling technologies, security and privacy, and applications," *IEEE Internet Things J.*, vol. 4, no. 5, pp. 1125–1142, Oct 2017.

[3] A. Zanella, N. Bui, A. Castellani, L. Vangelista, and M. Zorzi, "Internet of things for smart cities," *IEEE Internet Things J.*, vol. 1, no. 1, pp. 22–32, Feb 2014.

[4] Federal Communications Commission (FCC), *Connecting America: The national broadband plan.*, [Online]. Available: https://www.fcc.gov/general/national-broadband-plan, 2010.

[5] Defense Advanced Research Projects Agency (DARPA), *Shared spectrum access for radar and communications (SSPARC)*, [Online]. Available: http://www.darpa.mil/program/sharedspectrum-access-for-radar-and-communications, 2016.

[6] L. Zheng, M. Lops, Y. C. Eldar, and X. Wang, "Radar and communication coexistence: An overview: A review of recent methods," *IEEE Signal Process. Mag.*, vol. 36, no. 5, pp. 85–99, 2019.

[7] F. Liu, C. Masouros, A. P. Petropulu, H. Griffiths, and L. Hanzo, "Joint radar and communication design: Applications, state-of-the-art, and the road ahead," *IEEE Trans. Commun.*, vol. 68, no. 6, pp. 3834–3862, 2020.

[8] R. Saruthirathanaworakun, J. M. Peha, and L. M. Correia, "Opportunistic sharing between rotating radar and cellular," *IEEE J. Sel. Areas Commun.*, vol. 30, no. 10, pp. 1900–1910, 2012.

[9] A. Khawar, A. Abdelhadi, and C. Clancy, "Target detection performance of spectrum sharing MIMO radars," *IEEE Sensors J.*, vol. 15, no. 9, pp. 4928–4940, 2015.

[10] F. Liu, C. Masouros, A. Li, T. Ratnarajah, and J. Zhou, "MIMO radar and cellular coexistence: A power-efficient approach enabled by interference exploitation," *IEEE Trans. Signal Process.*, vol. 66, no. 14, pp. 3681–3695, 2018.

[11] F. Liu, L. Zhou, C. Masouros, A. Li, W. Luo, and A. Petropulu, "Toward dual-functional radar-communication systems: Optimal waveform design," *IEEE Trans. Signal Process.*, vol. 66, no. 16, pp. 4264–4279, 2018.

[12] C. G. Tsinos, A. Arora, S. Chatzinotas, and B. Ottersten, "Joint transmit waveform and receive filter design for dual-function radar-communication systems," *IEEE J. Sel. Topics Signal Process.*, pp. 1–1, 2021.

[13] F. Liu, C. Masouros, A. Li, H. Sun, and L. Hanzo, "MU-MIMO communications with MIMO radar: From co-existence to joint transmission," *IEEE Trans. Wireless Commun.*, vol. 17, no. 4, pp. 2755–2770, 2018.

[14] A. Kaushik, R. Singh, S. Dayarathna, R. Senanayake, M. Di Renzo, M. Dajer, H. Ji, Y. Kim, V. Sciancalepore, A. Zappone, and W. Shin, "Towards integrated sensing and communications for 6G: Key enabling technologies, standardization, and challenges," *IEEE Communications Standards Mag.*, In Press.

[15] A. Kaushik, R. Singh, M. Li, H. Luo, S. Dayarathna, R. Senanayake, X. An, R. A. S.-Gallacher, W. Shin, and M. Di Renzo, "Integrated sensing and communications for IoT: Synergies with key 6G technology enablers," *arXiv 2309.13542*, 2023.

[16] O. Dizdar, A. Kaushik, B. Clerckx, and C. Masouros, "Energy efficient dual-functional radar-communication: Rate-splitting multiple access, low-resolution DACs, and RF chain selection," *IEEE Open J. Commun. Society*, vol. 3, pp. 986–1006, 2022.

[17] X. Liu, T. Huang, N. Shlezinger, Y. Liu, J. Zhou, and Y. C. Eldar, "Joint transmit beamforming for multiuser MIMO communications and MIMO radar," *IEEE Trans. Signal Process.*, vol. 68, pp. 3929–3944, 2020.

[18] R. H. Walden, "Analog-to-digital converter survey and analysis," *IEEE J. Sel. Areas Commun.*, vol. 17, no. 4, pp. 539–550, Apr 1999.

[19] O. El Ayach, S. Rajagopal, S. Abu-Surra, Zhouyue Pi, and R. W. Heath, "Spatially sparse precoding in millimeter wave MIMO systems," *IEEE Trans. Wireless Commun.*, vol. 13, no. 3, pp. 1499–1513, March 2014.

[20] C. G. Tsinos, S. Maleki, S. Chatzinotas, and B. Ottersten, "On the energy-efficiency of hybrid analog-digital transceivers for single- and multi-carrier large antenna array systems," *IEEE J. Sel. Areas Commun.*, vol. 35, no. 9, pp. 1980–1995, Sept 2017.

[21] C. G. Tsinos, S. Chatzinotas, and B. Ottersten, "Hybrid analog-digital transceiver designs for multi-user MIMO mmWave cognitive radio systems," *IEEE Trans. Cogn. Commun. Netw.*, vol. 6, no. 1, pp. 310–324, March 2020.

[22] A. Kaushik, E. Vlachos, C. Tsinos, J. Thompson, and S. Chatzinotas, "Joint bit allocation and hybrid beamforming optimization for energy efficient millimeter wave MIMO systems," *IEEE Trans. Green Commun. Netw.*, vol. 5, no. 1, pp. 119–132, 2021.

[23] A. Kaushik, J. Thompson, E. Vlachos, C. Tsinos, and S. Chatzinotas, "Dynamic RF chain selection for energy efficient and low complexity hybrid beamforming in millimeter wave MIMO systems," *IEEE Trans. Green Commun. Netw.*, vol. 3, no. 4, pp. 886–900, 2019.

[24] A. Arora, C. G. Tsinos, B. S. M. R. Rao, S. Chatzinotas, and B. Ottersten, "Hybrid transceivers design for large-scale antenna arrays using majorization-minimization algorithms," *IEEE Trans. Signal Process.*, vol. 68, pp. 701–714, 2020.

[25] A. Kaushik, C. Masouros, and F. Liu, "Hardware efficient joint radar-communications with hybrid precoding and RF chain optimization," in *IEEE Int. Conf. Commun.*, 2021, pp. 1–6.

[26] A. Kaushik, E. Vlachos, C. Masouros, C. Tsinos, and J. Thompson, "Green joint radar-communications: RF selection with low resolution DACs and hybrid precoding," in *IEEE Int. Conf. Commun.*, 2022, pp. 3160–3165.

[27] O. E. Ayach, R. W. Heath, S. Abu-Surra, S. Rajagopal, and Z. Pi, "The capacity optimality of beam steering in large millimeter wave MIMO systems," in *IEEE 13th International Workshop on Signal Process. Advances in Wireless Commun. (SPAWC)*, June 2012, pp. 100–104.

[28] S. Domouchtsidis, C. G. Tsinos, S. Chatzinotas, and B. Ottersten, "Symbol-level precoding for low complexity transmitter architectures in large-scale antenna array systems," *IEEE Trans. Wireless Commun.*, vol. 18, no. 2, pp. 852–863, Feb 2019.

[29] S. Domouchtsidis, C. G. Tsinos, S. Chatzinotas, and B. Ottersten, "Joint symbol level precoding and combining for MIMO-OFDM transceiver architectures based on one-bit DACs and ADCs," *IEEE Trans. Wireless Commun.*, vol. 20, no. 7, pp. 4601–4613, 2021.

[30] C. G. Tsinos, S. Chatzinotas, and B. Ottersten, "RF precoding for cognitive radio systems," *IEEE Wireless Commun. Lett.*, vol. 11, no. 9, pp. 1845–1849, 2022.

[31] Foad Sohrabi and Wei Yu, "Hybrid beamforming with finite-resolution phase shifters for large-scale mimo systems," in *2015 IEEE 16th International Workshop on Signal Processing Advances in Wireless Communications (SPAWC)*, 2015, pp. 136–140.

[32] Mohammad Alaee-Kerahroodi, Mahmoud Modarres-Hashemi, and Mohammad Mahdi Naghsh, "Designing sets of binary sequences for mimo radar systems," *IEEE Transactions on Signal Processing*, vol. 67, no. 13, pp. 3347–3360, 2019.

[33] Qingqing Wu and Rui Zhang, "Beamforming optimization for wireless network aided by intelligent reflecting surface with discrete phase shifts," *IEEE Transactions on Communications*, vol. 68, no. 3, pp. 1838–1851, 2020.

[34] A. Kaushik, A. Arora, C. Tsinos, C. Masouros, F. Liu, and S. Chatzinotas, "Waveform design for joint radar-communications with low complexity analog components," in *2nd IEEE International Symposium Joint Commun. & Sensing (JC&S)*, 2022, pp. 1–5.

[35] S. Zhang and Y. Huang, "Complex quadratic optimization and semidefinite programming," *SIAM J. Optimization*, vol. 16, no. 3, pp. 871–890, 2006.

[36] D. P. Bertsekas, *Nonlinear programming*, Athena scientific, 1999.

[37] S. K. Mohammed and E. G. Larsson, "Per-antenna constant envelope precoding for large multi-user MIMO systems," *IEEE Trans. Commun.*, vol. 61, no. 3, pp. 1059–1071, March 2013.

[38] Daniel R. Fuhrmann and Geoffrey San Antonio, "Transmit beamforming for mimo radar systems using signal cross-correlation," *IEEE Transactions on Aerospace and Electronic Systems*, vol. 44, no. 1, pp. 171–186, 2008.

[39] Daniel R. Fuhrmann and Geoffrey San Antonio, "Transmit beamforming for MIMO radar systems using signal cross-correlation," *IEEE Trans. Aerosp. Electron. Syst.*, vol. 44, no. 1, pp. 171–186, 2008.

[40] C. G. Tsinos, A. A. Rontogiannis, and K. Berberidis, "Distributed blind hyperspectral unmixing via joint sparsity and low-rank constrained non-negative matrix factorization," *IEEE Trans. Comput. Imag.*, vol. 3, no. 2, pp. 160–174, 2017.

[41] C. G. Tsinos and B. Ottersten, "An efficient algorithm for unit-modulus quadratic programs with application in beamforming for wireless sensor networks," *IEEE Signal Proces. Letters*, vol. 25, no. 2, pp. 169–173, Feb 2018.

[42] C. G. Tsinos, S. Chatzinotas, and B. Ottersten, "Hybrid analog-digital transceiver designs for multi-user MIMO mmWave cognitive radio systems," *IEEE Trans. Cog. Commun. Netw.*, vol. 6, no. 1, pp. 310–324, 2020.

[43] V. Cevher, S. Becker, and M. Schmidt, "Convex optimization for big data: Scalable, randomized, and parallel algorithms for big data analytics," *IEEE Signal Process. Mag.*, vol. 31, no. 5, pp. 32–43, Sept 2014.

[44] Ernie Esser, Xiaoqun Zhang, and Tony F Chan, "A general framework for a class of first order primal-dual algorithms for convex optimization in imaging science," *SIAM J. on Imag. Sciences*, vol. 3, no. 4, pp. 1015–1046, 2010.

[45] E Gi Golshtein and NV Tretyakov, "Modified Lagrangians in convex programming and their generalizations," in *Point-to-Set Maps and Mathematical Programming*, pp. 86–97. Springer, 1979.

[46] Stephen Boyd, Neal Parikh, Eric Chu, Borja Peleato, and Jonathan Eckstein, "Distributed optimization and statistical learning via the alternating direction method of multipliers," *Foundations and Trends® in Machine Learning*, vol. 3, no. 1, pp. 1–122, 2011.

[47] S. Cui, A. J. Goldsmith, and A. Bahai, "Energy-constrained modulation optimization," *IEEE Trans. Wireless Commun.*, vol. 4, no. 5, pp. 2349–2360, Sept 2005.

[48] H. L. Van Trees, *Detection, estimation, and modulation theory, part I: detection, estimation, and linear modulation theory*, John Wiley & Sons, 2004.